JPEDAV (2008) 29:131–135
DOI: 10.1007/s11669-007-9244-1
1547-7037 ©ASM International

Homogenization of Highly Alloyed Cu-Fe-Ni: A Phase Diagram Study

Isabella Gallino, Stefano Curiotto, Marcello Baricco, Michael E. Kassner, and Ralf Busch

(Submitted August 16, 2007; in revised form October 31, 2007)

Six highly alloyed Cu-Fe-Ni alloys have been processed with different heat treatments and studied by means of electron microprobe and differential thermal analyses. The results are discussed in comparison with an equilibrium phase diagram calculation performed using the CALPHAD (CALculation of PHAse Diagrams) method. An unexpected temperature window for homogenization has been found in the middle of the composition range.

Keywords Cu-Fe-Ni, homogenization, phase diagram, CALPHAD

1. Introduction

Cu-Fe-Ni alloys have been recognized as a potential anode material for aluminum production.[1] This ternary alloy operates inertly during the electrolysis and produces pure oxygen as a by-product, in contrast to the consumable carbon anode of the Hall-Héroult process that produces undesirable greenhouse emissions such as carbon dioxide and perfluorocarbons. Although the aluminum inert-anode technology research has been focused on composite materials such as cermets,[2] the use of metals as nonconsumable anodes is preferred because of their high conductivity.

The recently proposed TiB_2 vertical cathode technology and the use of low-temperature slurry fluoride electrolytes[3] are intended to reduce the voltage required for the electrolysis and significantly reduce the operating temperature from 960 °C to as low as 750 °C. At these temperatures, metallic materials such as the Cu-Fe-Ni can be considered a valuable alternative to the carbon anode as well to the cermet inert anodes. In this respect, the assessment of the thermal stability of the Cu-Fe-Ni alloy system in the temperature range of 750 to 800 °C was the objective of this study. It led to unexpected results in disagreement with published phase diagrams of this system. Since the early investigations by Vogel[4] in 1910 and by Köster and Dannöhl in 1935,[5] there have been many theoretical and experimental investigations on Cu-Fe-Ni phase diagram.[6-13] However, the phase relationships at high temperatures (600-1200 °C) are not completely assessed, and some experimental results differ from the thermodynamic calculations. In 1990, Gupta[14] reported two calculated sections at 750 °C from different investigators,[6-7] which differ with each other. Ten years later, Qin et al. reported experimental isothermal sections in the range of 600 to 1050 °C.[11] These isotherms were determined using ternary diffusion couples and electron-probe microanalysis. In their work, the measured miscibility gap is somewhat smaller than all the previously calculated or experimentally assessed gaps. Furthermore, in 2001, Servant et al. reported the existence of an unexpected ternary-ordered phase $(Cu,Ni)_3Fe$[15] and recalculated the thermodynamic CALPHAD parameters.[12] Based on this model, one isopleth[16] and a few isothermal sections, at temperatures below 650 °C, have been recalculated.[12] The present investigation used the thermodynamic parameters of Servant et al.[12] to calculate the phase diagram in the range of 527 to 1127 °C and found that, for these temperatures, the new thermodynamic modeling still fails to correctly predict the phase equilibria. There is experimental evidence of a smaller miscibility gap and of a window of temperatures, in which Cu-Fe-Ni alloys can be unexpectedly homogenized into a single face-centered cubic (fcc) phase.

2. Experimental

Six highly alloyed Cu-Fe-Ni ternary alloys were produced by conventional casting of the elements (99.9% purity) into ingots of 5 cm diameter. The overall composition of the alloys is $Cu_x(Fe_{0.5}Ni_{0.5})_{1-x}$ where the mass fraction ratio of iron/nickel is fixed at 1/1, and the mass fraction of copper x varies as 0.1, 0.2, 0.3, 0.4, 0.6, and 0.7. The compositions of the as-cast samples in weight and atomic percent are listed in Table 1. The material has been examined with a CAMECA (Gennevilliers, France) model SX50 electron microprobe analyzer (EMPA) with wavelength dispersive spectrometer, operated with a beam current of 49.53 nA, an accelerating voltage of 15.1 kV,

Isabella Gallino and **Ralf Busch,** Department of Mechanical Engineering, Oregon State University, 204 Rogers Hall, Corvallis, OR 97331; **Isabella Gallino** and **Ralf Busch,** Department of Materials Science and Engineering, Saarland University, Campus C6.3, 66123 Saarbrücken, Germany; **Stefano Curiotto** and **Marcello Baricco,** Department of Chemistry I.F.M. and NIS, University of Turin, via P. Giuria 9, 10125 Torino, Italy; and **Michael E. Kassner,** Department of Aerospace and Mechanical Engineering, University of Southern California, Los Angeles, CA 90089. Contact e-mail: i.gallino@mx.uni-saarland.de.

and a take-off angle of 40°. The samples were coated with carbon and ground after mechanical polishing. The EMPA was calibrated using pure metal standards and quartz for oxygen. The counting times were 10 s on the Kα peak of each element and 5 s on each background. The backgrounds were taken at 500 sin θ off-peak with the exception of oxygen, which had a background shift of 3000 sin θ. The diffracting crystals were Li-F to detect Fe, Ni, and Cu, and PC1 for O. Standard ZAF corrections were applied. A reproducibility test was also conducted by taking 10 measurements in the same location of a sample. The counting statistics for each element are in mass fraction 0.023, 0.10, 0.12, and 0.18 for O, Fe, Ni, and Cu, respectively. A CAMSCAN-FE scanning electron microscope (SEM) by CAMSCAN Ltd. (Waterbeach, Cambridgeshire, UK), operated at 20 kV, was used to photograph the decomposed microstructures. A Perkin-Elmer differential thermal analyzer (DTA), calibrated with In, Zn, Al, Ag, and Ni, was used to study the thermal stability of the alloys. The samples were heated in high-purity graphite crucibles in a flux of argon to 1600 °C with a constant heating rate of 0.33 K/s and cooled back to room temperature at the same rate.

3. Results and Discussion

The microstructure of the $Cu_x(Fe_{0.5}Ni_{0.5})_{1-x}$ alloys after casting consists of iron-nickel-rich dendrites embedded in a copper-rich matrix. The microstructure features decrease in size with increasing copper content in the alloy. Figure 1(a) shows the case for the as-cast alloy with $x = 0.6$. Here, the backscattering electrons (BSE) show a matrix that appears bright in contrast to the darker dendritic structures. The black spots are dispersed oxide particles, identified by EMPA as Fe_3O_4. This alloy has an overall composition Cu/Fe/Ni of 60/20/20 wt%, equivalent to 57.5/21.8/20.7 at.%, and the EMPA detected a Cu-enriched matrix (Fe and Ni-depleted) with concentration of Cu/Fe/Ni of 81/8/11 at.%. The matrix is therefore a soft phase rich in copper. The as-cast material has yield strength values similar to that of pure copper (25.5 MPa at a strain of 0.05 in tension) and exhibits some ductile behavior (elongation = 5%).[17] The dendrites have a core much richer in iron and nickel and poorer in copper than the matrix. For example, the concentration in the dendrite core for the $x = 0.6$ alloy was detected, on average, as 24/45/31 at.%. Based on tensile tests and DTA of the as-cast materials, the dendrites showed brittle failure and melted at high temperatures, up to 1390 °C.[17] Coring is visible at high magnifications using optical microscopy. For the alloy in Fig. 1(a), linear traversal microprobe chemical analyses detected that the composition gradually changes from the core of the dendrite to the outer shell from 24/45/31 to 38.4/34/27.6 at.%.

Such coarse inhomogeneous microstructures are undesirable for use as anode material. The as-cast microstructure leaves large areas of the surface highly concentrated in copper (the matrix) exposed to the corrosive electrolyte. A homogeneous or finely decomposed structure is expected to be more resistant to attack. For this reason, the present study aimed to develop a method to homogenize all of the as-cast microstructures. A heat treatment at 1100 °C for 12 h in a 10^{-2} Pa vacuum furnace successfully homogenized all of the compositions. Figure 1(b) shows the BSE image for the alloy with $x = 0.6$ after this treatment. The microstructure transformed from dendritic into a homogeneous microstructure consisting of equiaxed grains (single γ-phase). The previous locations of the dendrites are still slightly detectable at places as darker areas. Nevertheless, the measured concentration of copper, nickel, and iron is equal to the overall concentration with relatively small fluctuations, at

Table 1 Alloy compositions in wt% and at.% for $Cu_x(Fe_{0.5}Ni_{0.5})_{1-x}$

x	Cu/Fe/Ni, wt%	Cu/Fe/Ni, at.%
0.1	10/45/45	9.1/46.6/44.3
0.2	20/40/40	18.4/41.8/39.8
0.3	30/35/35	27.8/37/35.2
0.4	40/30/30	37.5/32/30.5
0.6	60/20/20	57.5/21.8/20.7
0.7	70/15/15	67.8/16.5/15.7

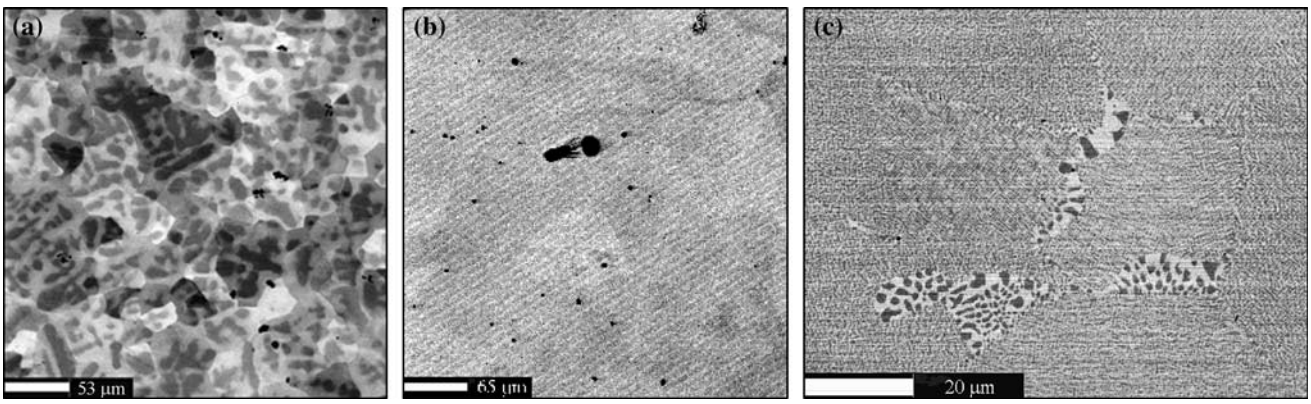

Fig. 1 BSE-images of $Cu_x(Fe_{0.5}Ni_{0.5})_{1-x}$ with mass fraction $x = 0.6$. (a) As-cast alloy. (b) After 12 h at 1100 °C followed by water quenching. (c) As-homogenized alloy after 400 h at 750 °C

about 1 to 2 at.%. Small-angle neutron scattering (SANS) analyses, performed on the alloy $x = 0.7$ after the heat treatment at 1100 °C, revealed that spinodal decomposition of the γ-phase occurred during cooling, despite careful water quenching.[17] The composition wavelength of the decomposed γ-phase was found to be 63 nm.

After the homogenization treatment, followed by quenching, the alloys were equilibrated at 750 and 800 °C for 400 h in the vacuum furnace. Upon annealing, discontinuous coarsening reactions originate at the grain boundaries of the original γ-grains. The microstructure of the $x = 0.6$ alloy after 400 h at 750 °C is shown in Fig. 1(c). Here, segments of the grain boundaries of the original γ-phase have migrated and consumed the matrix, leaving behind large cellular-shape particles, which are typical for continuous coarsening. The remaining matrix, which was already spinodally decomposed, also coarsened, but at a slower rate. The new phases are chemically different fcc solid solutions, one enriched in nickel and iron, γ_1, and the other in copper, γ_2. The discontinuous coarsening occurred in all of the as-homogenized compositions with the exception of alloys with $x = 0.1$ at 750 °C, and $x = 0.1$ and 0.2 at 800 °C, indicating that, at these temperatures, these compositions lie outside the gap. In contrast, the as-cast alloys that did not undergo the homogenization pretreatment preserved the two-phase dendritic microstructure even after 400 h at 750 and 800 °C.[17]

Figure 2 shows the DTA curves for the as-homogenized alloys with mass fraction $x = 0.4$, 0.6, and 0.7. On heating, these alloys show a small exothermic event (signal I) that was not detected for as-cast alloys and that corresponds to the crossing of the solvus line. The solvus temperature was taken as the onset of signal I. As the copper content in the alloy increases from $x = 0.1$ to 0.7, the solvus temperature increases gradually from 590 to 1055 °C, the onset of melting is reduced from 1392 to 1151 °C, and the melting transformation goes from a single event process to a multiple event. In fact, the Cu-poor alloys ($x = 0.1$, 0.2, and 0.3) produced DTA curves with single melting and single solidification peaks.[17] The alloy with $x = 0.4$ shows two melting events with heating, a signal II, slightly visible in Fig. 2, and a large signal III, and shows two exothermic peaks on cooling. The $x = 0.6$ and 0.7 alloys show multiple melting events on both heating and cooling (signals II, III, IV, and V that has a distinct shoulder), indicating that a ternary peritectic reaction takes place in this region of the phase diagram. Each of these signals indicates one step of the ternary peritectic melting of the γ_2 phase that transforms into (liquid + γ_2), then into (liquid + γ_2 + γ_1), then into (liquid + γ_1), to finally reach the liquid region.

The isopleth along the Fe/Ni ratio of 1/1 was calculated using the CALPHAD parameters of Servant et al.,[12] and it is plotted in Fig. 3. The temperature is plotted, by means of the Thermocalc software, against the mass fraction of Cu in the ternary alloy. The calculated miscibility gap (γ_1 + γ_2 field) gets smaller with increasing temperature until it culminates into a ternary peritectic. For comparison, the solid symbols represent readings from the isopleths published by Köster and Dannöhl,[5] and good agreement exists between the solids symbols and the calculated isopleth. Our

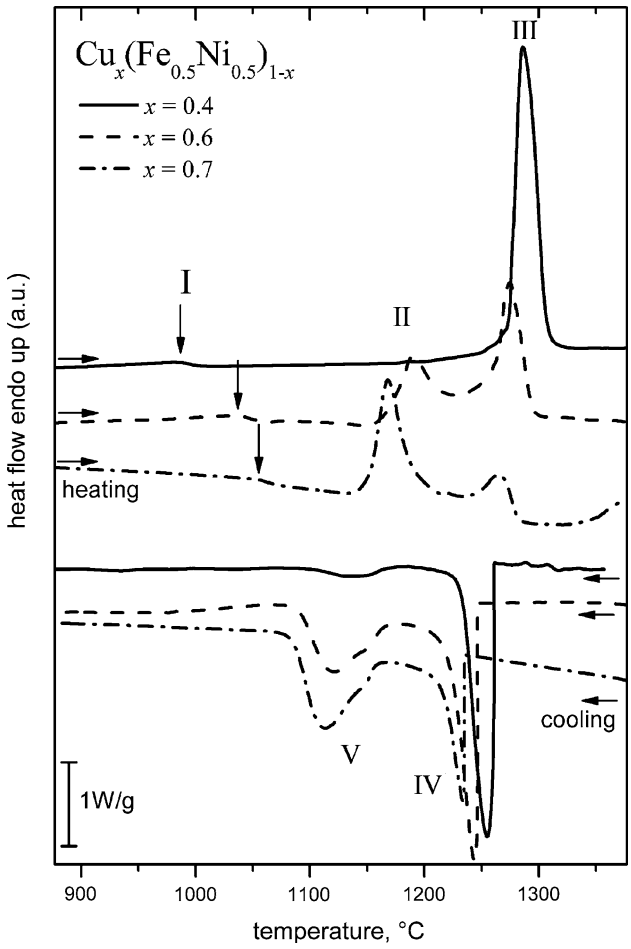

Fig. 2 DTA curves of the heat flow versus temperature at scanning rate of 0.33 K/s for the homogenized $Cu_x(Fe_{0.5}Ni_{0.5})_{1-x}$ with mass fraction $x = 0.4$, 0.6, and 0.7. I indicates the solvus event, which onset is indicated with an arrow; II and III the melting events; IV and V the solidification events

DTA results on the homogenized alloys are plotted in Fig. 3 as open symbols. For each of the studied compositions, the circles represent the liquidus curve (peak temperature of signal III), the triangles the solidus curve (onset of signal II), and the open hexagonal symbols the solvus line (onset of signal I). The DTA data for the solvus are in agreement with the calculated miscibility gap and with the Köster- Dannöhl data only for alloys compositions 0.1, 0.2, and 0.3. The fact that the experimental solvus temperature for the compositions 0.4, 0.6, and 0.7 lies at considerably lower temperature than expected based on the thermodynamic model is in agreement with the observation that these alloys were successfully homogenized at 1100 °C.

According to the calculated phase diagram of Fig. 3 and the literature,[4-15] the homogenization for the composition $x = 0.6$ and 0.7 is particularly unexpected. These two compositions lie within the calculated miscibility gap until the peritectic melting, and the as-cast microstructure was expected to be retained after the heat treatment at 1100 °C. Instead, the microstructure transformed into a homogeneous

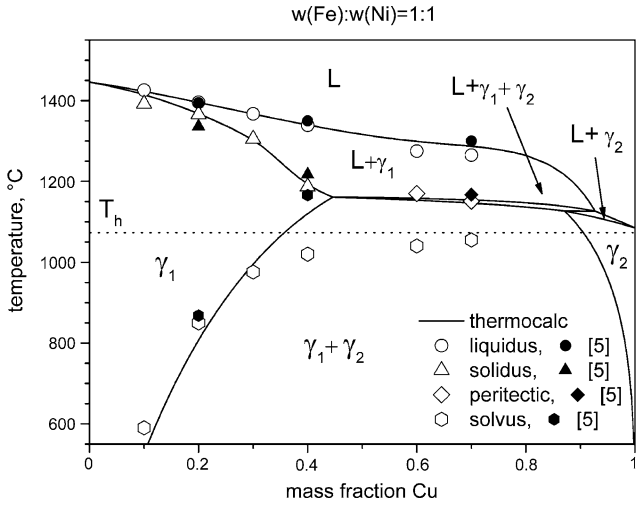

Fig. 3 Calculated isopleth for Cu-Fe-Ni for the mass fraction ratio Fe/Ni = 1/1. The open symbols represent our DTA data, the solid symbols are data taken from Ref 5. The temperature at which the sample could be successfully homogenized is indicated as T_h

structure, and upon quenching and equilibrating at 750 and 800 °C, spinodal decomposition and discontinuous coarsening took place. According to our DTA results, a narrow temperature window exists between solvus and solidus surfaces in which all our six alloys can be homogenized into a single γ-phase. To prevent local melting of the Cu-rich matrix, a homogenization temperature below the melting point of pure Cu is preferred. For Fig. 3, this temperature lies at 1073 °C.

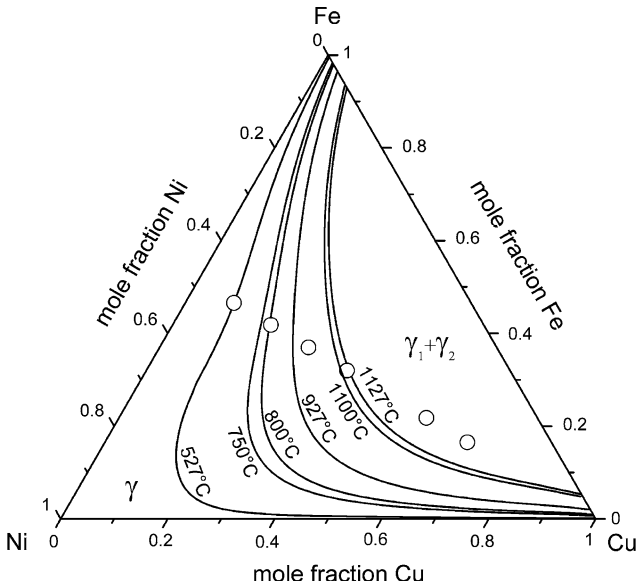

Fig. 4 Projections of the calculated miscibility gap for Cu-Fe-Ni at temperatures ranging from 527 to 1127 °C. The open circle symbols represent the studied alloy compositions. For simplification, the tie-lines, the Fe-rich bcc phase, and the melting reactions are not plotted

The isopleth of Fig. 3 is useful to describe phase transformations at fixed alloy compositions and to discuss the DTA results, but it should be noted that the figure does not represent the phase equilibria exactly. In fact, the 1/1 ratio of Fe/Ni does not follow any of the equilibrium tie-lines for this ternary miscibility gap. The tie-lines are tilted with respect to this ratio because of an unequal chemical interaction between Cu and Fe versus Cu and Ni, that is, a repulsive chemical interaction between Cu and Fe atoms, and a less strong repulsive interaction between Cu and Ni atoms. The tie-lines also change direction with alloy composition and with temperature. For this reason, several isothermal sections and respective tie-lines were calculated using the CALPHAD parameters described previously. Figure 4 shows the projections of the miscibility gap surface calculated at temperatures between 527 and 1127 °C. Here, the miscibility gap gets smaller with increasing temperature, gradually leaving outside the studied $Cu_x(Fe_{0.5}Ni_{0.5})_{1-x}$ compositions plotted as open circles. At 1100 °C, the calculation depicts the alloys with mass fraction $x = 0.4$, 0.6, and 0.7 still within the miscibility gap. Only a slightly larger solubility of Cu than the one thermodynamically calculated, or a small confinement of the gap on the Cu-rich side, would bring these compositions outside the miscibility gap. Based on this observation, the discrepancy between the calculated miscibility gap and our experimental DTA solvus values is not as large as it appears in Fig. 3.

Moreover, Fig. 5 and 6 show the calculated isothermal section for 750 and 800 °C, respectively, including the calculated tie-lines (dotted lines) and the body-centered cubic (bcc) phase in the Fe-rich region. The triangle symbols represent the average chemical composition detected by EMPA for γ_1 and γ_2 for the alloys with overall composition $x = 0.4$ and 0.7 (circle symbols). The experimental tie-line (dashed line) is in agreement with the calculated tie-lines, although the detected composition for γ_2 (Cu-rich phase) is less enriched in Cu than that calculated.

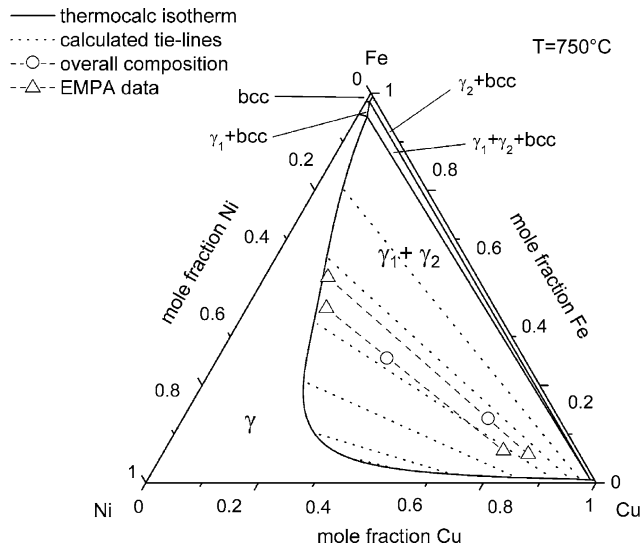

Fig. 5 Calculated isothermal gap for the Cu-Fe-Ni system at 750 °C

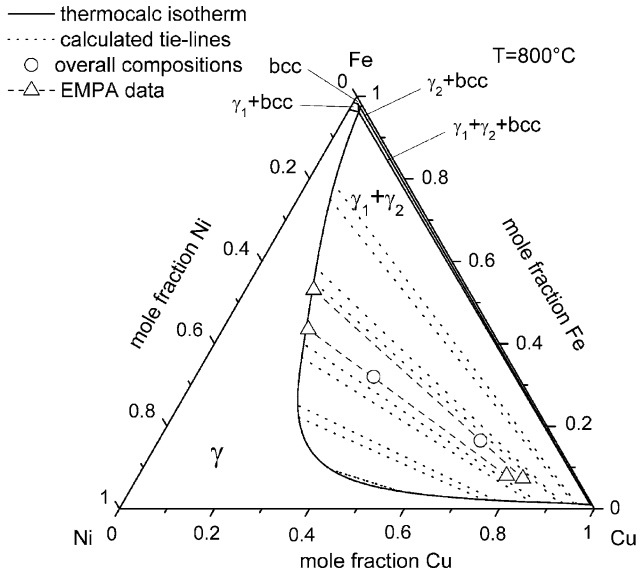

Fig. 6 Calculated isothermal gap for the Cu-Fe-Ni system at 800 °C

When compared with the work of Qin et al.,[11] our EMPA composition data lie on their measured miscibility gap. The thermodynamic calculation of the phase diagram always overestimated the size of the $\gamma_1 + \gamma_2$ miscibility gap especially on the Cu-rich side, but agree with all the previous calculated miscibility gaps particularly those calculated by Spencer et al.,[8] Chuang et al.,[9] and the most recent assessment by Wang et al.[13]

4. Conclusions

The miscibility gap for the Cu-Fe-Ni system is found experimentally smaller than the one obtained by thermodynamic calculations. The most important result is the finding of an unexpected window of temperatures, in which the $Cu_x(Fe_{0.5}Ni_{0.5})_{1-x}$ alloys can be successfully homogenized into a single γ-phase. Our experimental results appear in agreement with the experimental work of Qin et al.,[11] whereas the CALPHAD calculation may overestimate the size of the $\gamma_1 + \gamma_2$ miscibility gap, especially at high temperatures on the Cu-rich side.

Acknowledgment

The work has been supported by the Oregon Metals Initiative.

References

1. T.M. Van Leeuwen, "An Aluminum Revolution," Equity Research Report, Boston MA: Credit Suisse First Boston Corporation, June 22, 2000
2. D.R. Sadoway, Inert Anodes for the Hall-Heroult Cell: The Ultimate Materials Challenge, *JOM*, 2001, **53**(5), p 34-35
3. C.W. Brown, Next Generation Vertical Electrode Cells, *JOM*, 2001, **53**(5), p 39-42
4. R. Vogel, On the Ternary System: Iron-Copper-Copper, *Z. Anorg. Chem.*, 1910, **67**, p 1-17, (in German)
5. V.W. Köster and W. Dannöhl, The System Copper-Nickel-Iron, *Z. Metallkd.*, 1935, **27**, p 220-226, (in German)
6. A.J. Bradley, W.C. Cox, and H.J. Goldschmidt, An X-Ray Study of the Iron-Copper-Nickel Equilibrium Diagram at Various Temperatures, *J. Inst. Met.*, 1941, **67**, p 189-201
7. Y.A. Chang, J.P. Neumann, A. Mikula, and D. Goldberg, *Phase Diagrams and Thermodynamic Properties of Ternary Copper-Metal Systems*, INCRA Monograph, International Copper Research Association, 1979
8. P. Spencer, K. Hack, Z. Moser, and W. Zakulski, Calculation of the FCC/Liquid Phase Equilibria in the Fe-Cu-Ni System, *Calphad*, 1985, **9**(2), p 191-198
9. Y.Y. Chuang, R. Schmid, and Y.A. Chang, Calculation of the Equilibrium Phase Diagrams and the Spinodally Decomposed Structures of the Cu-Ni-Fe System, *Acta Metall.*, 1985, **33**(8), p 1369-1385
10. K.J. Rönkä, A.A. Kodentsov, P.J.J. van Loon, J.K. Kivilahti, and F.J.J. van Loo, Thermodynamic and Kinetic Study of Diffusion Paths in the System Cu-Fe-Ni, *Metall. Mater. Trans. A*, 1996, **27A**, p 2229-2238
11. G.W. Qin, G. Zhao, M. Jiang, H.X. Li, and S.M. Hao, The Isothermal Sections of the Fe-Cu-Ni Ternary System at 600, 800, 1000, and 1050 °C, *Z. Metallkd.*, 2000, **91**(5), p 379-382
12. C. Servant, B. Sundman, and O. Lyon, Thermodynamic Assessment of the Cu-Fe-Ni System, *Calphad*, 2001, **25**(1), p 79-95
13. C.W. Wang, X.J. Liu, I. Ohnuma, R. Kainuma, and K. Ishida, Thermodynamic Database of the Phase Diagram in Cu-Fe Base Ternary Systems, *J. Phase Equilib. Diffus.*, 2004, **25**, p 320-328
14. K.P. Gupta, *Phase Diagrams of Ternary Nickel Alloys*, Part I, The Indian Institute of Metals, 1990
15. C. Servant, M. Guymont, and O. Lyon, A New Phase in the Ternary System Cu-Fe-Ni, *Scr. Mater.*, 2001, **45**, p 103-108
16. M. Baricco, E. Bosco, G. Acconciaioco, P. Rizzi, and A. Coisson, Rapid Solidification of Cu-Fe-Ni Alloys, *Mater. Sci. Eng. A*, 2004, **Sp. Iss. SI 375**, p 1019-1023
17. I. Gallino, "Phase Diagram, Thermal Stability and High Temperature Oxidation of the Ternary Cu-Ni-Fe System," Ph.D. thesis, Oregon State University, 2004